arXiv:1405.7314v1 [quant-ph] 28 May 2014

Entanglement Dynamics in the Presence of Controlled Unital Noise

A. Shaham, A. Halevy, L. Dovrat, E. Megidish, and H. S. Eisenberg

Racah Institute of Physics, Hebrew University of Jerusalem, Jerusalem 91904, Israel

Quantum entanglement is notorious for being a very fragile resource. Significant efforts have been put into the study of entanglement degradation in the presence of a realistic noisy environment. Here, we present a theoretical and an experimental study of the decoherence properties of entangled pairs of qubits. The entanglement dynamics of maximally entangled qubit pairs is shown to be related in a simple way to the noise representation in the Bloch sphere picture. We derive the entanglement level in the case when both qubits are transmitted through any arbitrary unital Pauli channel, and compared it to the case when the channel is applied only to one of the qubits. The dynamics of both cases was verified experimentally using an all-optical setup. We further investigated the evolution of partially entangled initial states. Different dynamics was observed for initial mixed and pure states of the same entanglement level.

PACS numbers: 03.65.Yz, 03.67.Mn, 42.25.Ja, 42.50.Lc, 42.79.-e

I. INTRODUCTION

Quantum entanglement is an essential ingredient in many quantum information tasks. It is vital for the implementation of quantum protocols such as quantum teleportation and dense coding, as well as for other computational schemes [1]. Decoherence – the undesired coupling of a quantum system to other non-accessible systems, results in quantum noise which reduces the degree of entanglement that the system of interest possesses. This in turn can hinder the success of quantum information protocols. Therefore, the characterization of entanglement dynamics under the influence of decohering processes is required for any future realization of these quantum information applications.

There are two main approaches for studying the dynamics of entanglement. In the first, a specific model which is a result of a specific physical implementation of noise is considered [2–5]. In the second approach, dynamics is studied more generally, based on the knowledge of the noise parameters and the initial state [6–9]. Some previous works have focused on the specific moment where entanglement disappears, referring to it as the sudden death point if entanglement vanishes while local coherence still prevails [10, 11]. Other works addressed a more general binary question: does a given noisy channel preserve or break entanglement? [12–14]. Among the above works, a few have dealt with the case where the noise is unital, i.e., mapping the maximally mixed state onto itself. [2, 12–14].

In this work, we investigate the entanglement dynamics of qubit pairs transmitted through controlled uncorrelated and local unital noisy channels. The dynamics of two maximally entangled qubits that are both affected by the channel is derived. We show that the entanglement level of the system, quantified by the concurrence measure, is described by simple relations of the important parameters of the noise. These relations are verified experimentally using an all-optical setup. Furthermore, by generating different initial states, it is shown how entanglement evolution is affected by the amount of entanglement in the initial state, and its mixedness.

II. THEORETICAL MODEL

The entanglement of a qubit pair is commonly quantified using the concurrence measure [15] defined as $C(\hat{\rho}) = \max\{0, Q(\hat{\rho})\}$, where $Q = \sqrt{\lambda_0} - \sqrt{\lambda_1} - \sqrt{\lambda_2} - \sqrt{\lambda_3}$, λ_i are the ordered positive eigenvalues of $\Lambda = \hat{\rho}(\sigma_y \otimes \sigma_y)\hat{\rho}^*(\sigma_y \otimes \sigma_y)$, $\hat{\rho}^*$ is the complex conjugate of the density matrix $\hat{\rho}$ of the state in the computational basis and σ_y is the second Pauli matrix. The concurrence is one for maximally entangled states such as the Bell states $|\psi^{\pm}\rangle = (|01\rangle \pm |10\rangle)/\sqrt{2}$ and $|\phi^{\pm}\rangle = (|00\rangle \pm |11\rangle)/\sqrt{2}$, and zero for separable states.

Consider a quantum channel that acts on a single-qubit state $\hat{\rho}$. The operation of the channel can be uniquely described by a completely positive map $\mathcal{E}$, using the elements of the process matrix χ

$$\mathcal{E}(\hat{\rho}) = \sum_{m,n} \chi_{mn} \hat{E}_m \hat{\rho} \hat{E}_n^{\dagger}, \tag{1}$$

where $\hat{E}_m$ are called Kraus operators and span the vector space of $\hat{\rho}$. χ is positive, Hermitian, and satisfies $\mathrm{Tr}(\chi) = 1$ (i.e., the channel is nondissipative). In the case of a quantum system in n-dimensional Hilbert space, χ is a $n^2 \times n^2$ matrix. In addition, the channel can be geometrically represented as the mapping of the surface of the Bloch sphere onto a smaller contained ellipsoid surface [1].

If the channel is unital (i.e., $\mathcal{E}(\hat{I}) = \hat{I}$), the sphere surface and the mapped ellipsoid are concentric. As was shown in Ref. 16, the mapping operation of unital channels can be understood as the implementation of two unitary rotations $\{U, V\}$, along with a three-parameter simpler map $\mathcal{E}_D$:

$$\mathcal{E}(\hat{\rho}) = U\mathcal{E}_D(V\hat{\rho}V^{\dagger})U^{\dagger}. \tag{2}$$

The map $\mathcal{E}_D$ can be described using three parameters $\{R_1, R_2, R_3\}$, which are the lengths of the primary axes of the mapped ellipsoid. For unital channels, the process matrix that describes the $\mathcal{E}_D$ operation is χ_D, the diagonalization of the process matrix χ. The radii $\{R_1, R_2, R_3\}$ are related to the eigenvalues of χ by

$$R_i = \chi_0 + \chi_i - \chi_j - \chi_k \,, \tag{3}$$

where $i \neq j \neq k \neq 0$ [16]. A negative value of R_i is interpreted as an inversion of the mapped ellipsoid with respect to a plane perpendicular to R_i. The complete positivity of χ is equivalent to the requirements that $|R_i \pm R_j| \leq |1 \pm R_k|$ [16]. These inequalities define an allowed tetrahedral volume within the three dimensional radii space [16].

A unital channel that does not include rotations (i.e., $U = V = I$) is called a Pauli channel. When the $\hat{E}$ matrices are the σ_0 identity matrix and the σ_1, σ_2, and σ_3 Pauli matrices, the χ matrix that describes the Pauli channel is the diagonal χ_D matrix. Denoting the correseponding eigenvalues of χ_D by $\{\chi_0, .., \chi_3\}$, we write the probability for a change in the initial state as

$$P = \sum_{i=1}^{3} \chi_i = 1 - \chi_0 \,. \tag{4}$$

We analyze the case when a qubit pair is initially prepared in a maximally entangled Bell state $|\psi_B\rangle$. A unital Pauli channel, which is designated by the symbol \$ and represented by a diagonal matrix χ_D, is then applied with a probability P to one of the two qubits (i.e., $\mathcal{E} = (I \otimes \$)$). Calculating the output state $\mathcal{E}(|\psi_B\rangle\langle\psi_B|)$ using Eq. (1), we obtain that the eigenvalues of the corresponding $\Lambda[(I \otimes \$)|\psi_B\rangle\langle\psi_B|]$ matrix are $\{\chi_0^2, \chi_1^2, \chi_2^2, \chi_3^2\}$. If $\lambda_0 = \chi_0^2$ is the maximal eigenvalue, the concurrence in terms of P is written using Eq. 4 as: $C = \max\{\chi_0 - \chi_1 - \chi_2 - \chi_3, 0\} = \max\{1 - 2P, 0\}$.

Rewriting the concurrence as a function of the primary radii R_i, we obtain: $C = \max\{(R_1 + R_2 + R_3 - 1)/2, 0\}$. Generalizing this relation to the case where the maximal eigenvalue of Λ is not λ_0, the concurrence becomes

$$C[\mathcal{E}(|\psi_B\rangle\langle\psi_B|)] = \max\{(|R_1| + |R_2| + |R_3| - 1)/2, 0\}. \tag{5}$$

This equation describes the concurrence evolution when the noise is unital [13]. An immediate result from Eq. (5) is the entanglement breaking condition [12]: entanglement disappears when the channel satisfies $|R_1| + |R_2| + |R_3| \leq 1$. As unitary local rotations do not change the amount of entanglement, Equation (5) is valid not just for the Bell states, but also for any maximally entangled initial state.

A second situation that we would like to study is when the same local unital Pauli process \$ is applied to both qubits of $|\psi_B\rangle$ (i.e., $\mathcal{E} = (\$ \otimes \$)$). Calculating the concurrence of the output state as a function of the eigenvalues of χ $\{\chi_0, .., \chi_3\}$, we find that the eigenvalues of $\Lambda[(\$ \otimes \$)|\psi_B\rangle\langle\psi_B|]$ are

$$\begin{aligned} \lambda_0 &= (\chi_0^2 + \chi_1^2 + \chi_2^2 + \chi_3^2)^2, \\ \lambda_1 &= 4(\chi_1\chi_2 + \chi_3\chi_0)^2, \\ \lambda_2 &= 4(\chi_1\chi_3 + \chi_2\chi_0)^2, \\ \lambda_3 &= 4(\chi_1\chi_0 + \chi_2\chi_3)^2. \end{aligned} \tag{6}$$

λ_0 is the maximal eigenvalue of Λ. Substituting the values of R_i from Eq. (3) results with the output state concurrence

$$C[\mathcal{E}(|\psi_B\rangle\langle\psi_B|)] = \max\{(R_1^2 + R_2^2 + R_3^2 - 1)/2, 0\}. \tag{7}$$

Notice the similarity between our result of Eq. (7) and the former result of Eq. (5). Accordingly, the entanglement breaking condition in the last case is $R_1^2 + R_2^2 + R_3^2 \leq 1$. This condition was reported in [14] as applicable to the case of unital channels that are applied on both qubits of any entangled state. Unlike Eq. (5), the entanglement dynamics described by Eq. (7) does not apply to *any* unital channel and to *any* maximally entangled initial state. Numerical simulations suggest that in the general case where the unital channel is not a Pauli channel, the loss of entanglement is faster, and $(R_1^2 + R_2^2 + R_3^2 - 1)/2$ is only an upper bound for the concurrence. This was only proved for the entanglement breaking point, but not for channels that may leave the state partially entangled [14]. Equation (7) does hold in some cases, such as when the noise is isotropic ($R_1 = R_2 = R_3$, as will be shown below) and the initial state is any maximally entangled state, or for any unital noise when the initial state is the singlet state $|\psi^-\rangle$.

III. EXPERIMENTAL SETUP

In order to study entanglement dynamics experimentally, we generated entangled pairs of photons, transmitted them through controllable unital noisy channels, and measured the final concurrence of the output states. Entanglement was formed between the polarization degrees of freedom (DOFs), where the horizontal $|h\rangle$ and the vertical $|v\rangle$ polarization modes define the computational basis. The experimental setup is shown in Fig. 1(a): Photon pairs are collinearly generated by the process of spontaneous parametric down conversion. Using a lens of 30 cm focal length (L1), a pulsed 390 nm pump laser is focused onto two perpendicularly oriented 1 mm thick type-I $\beta - BaB_2O_4$ (BBO) crystals. After the crystals, the down-converted signal is separated from the pump beam using a dichroic mirror (DM). A half-wave plate (HWP) at an angle of δ is placed before the generating crystals in order to control the relative pump power of each crystal. Thus, the generated state is $|\psi\rangle = \cos(2\delta)|hh\rangle + \sin(2\delta)e^{i\varphi}|vv\rangle$. The angle φ is controlled by tilting another compensating crystal which is placed after the generating crystals. Before entering the quantum channel, the state is filtered spatially using a single-mode fiber (SM), and spectrally by a 3 nm

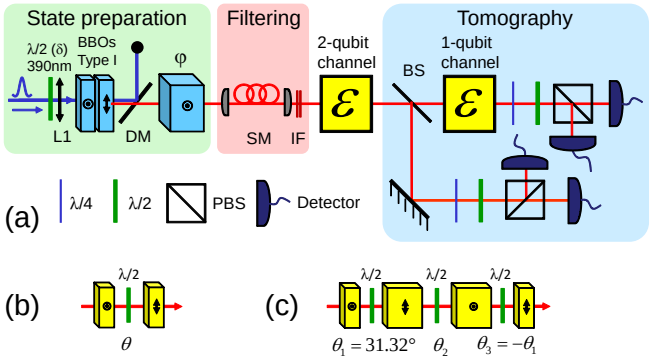

FIG. 1. (color online) The experimental setup. (a) State generation and characterization units: photon pairs are generated in the BBO crystals, which are located after a lens (L1) and a half-wave plate (HWP, $\lambda/2$) in an angle of δ. The down-converted signal passes through a dichroic mirror (DM), a birefringent compensating crystal (φ), a single-mode fiber (SM), and a 3 nm interference bandpass filter (IF). In the state characterization unit, the photons are split probabilistically by a beam splitter (BS) to two ports. In each port, the photons pass a sequence of a quarter-wave plate ($\lambda/4$), a HWP, and a polarizing beam splitter (PBS) before being coupled into single-photon detectors. (b) The two-field channel, composed of two perpendicularly oriented identical 2 mm thick calcite crystals. (c) The three-field (isotropic) channel. This channel is composed of four crystals and two fixed HWPs. The thickness of the two outer (inner) crystals is 1 mm (2 mm).

interference bandpass filter (IF). In the state characterization unit, the photons are first split probabilistically by a beam splitter (BS). Then, their post-selected two-port polarization state is measured by a two-qubit quantum state tomography procedure [17]. The required projections are achieved by wave-plates and polarizing beam splitters (PBS) that are placed before the single-photon detectors of each port.

Controlled quantum channels were implemented using a sequence of fixed birefringent calcite crystals and HWPs [18, 19] (see Fig. 1(b),(c)). Each crystal entangles the polarization modes of a photon with its internal temporal DOFs. Decoherence occurs when the photon detection is insensitive to the temporal delays, practically averaging over these DOFs. In order to apply a channel to one of the qubits we placed it in one port after the BS. A two-qubit channel was realized by placing the channel before the BS. For both channel types, control over the noise probability P was achieved by rotating the corresponding HWPs to different angle settings [19].

Two different unital channels were implemented. The first is the two-field channel [19, 20], (see Fig. 1(b)). It is described by random, but equally probable σ_1 or σ_2 rotations of the initial state, with overall noise probability of P

$$\mathcal{E}(\hat{\rho}) = (1-P)\hat{\rho} + \frac{P}{2}\sigma_1\hat{\rho}\sigma_1 + \frac{P}{2}\sigma_2\hat{\rho}\sigma_2\,. \qquad (8)$$

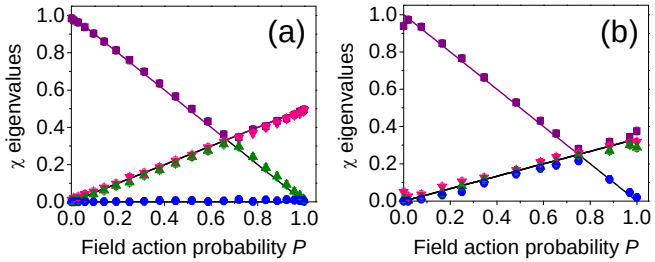

FIG. 2. (color online) Channel characterization. Measured eigenvalues of the process matrices for the (a) two-field and (b) the isotropic channels as a function of the noise probability P, with their theoretical predictions (solid lines).

Substituting the process matrix eigenvalues $\{1-P, \frac{P}{2}, \frac{P}{2}, 0\}$ in Eq. (3), we find that the primary radii of the mapped ellipsoid follows $\{R_1 = R_2, R_3 = 2R_1 - 1\}$. The second channel is an isotropic depolarization channel [21] (see Fig. 1(c)). It is described as

$$\mathcal{E}(\hat{\rho}) = (1-P)\hat{\rho} + \frac{P}{3}\sigma_1\hat{\rho}\sigma_1 + \frac{P}{3}\sigma_2\hat{\rho}\sigma_2 + \frac{P}{3}\sigma_3\hat{\rho}\sigma_3\,. \qquad (9)$$

The eigenvalues of the single-qubit process matrix of these channels, as obtained with a quantum process tomography procedure are presented in Figs. 2(a) and 2(b). The noise probability P is controlled by the rotation of the corresponding channel wave-plate. Surprisingly, for both channels $P = \sin^2(2\theta)$, where for the isotropic channel $\theta = \theta_2$. Errors are calculated using a maximal likelihood procedure and Monte Carlo simulations, assuming Poissonian noise [17, 20].

IV. DYNAMICS OF MAXIMALLY ENTANGLED STATES

Setting $\delta = 22.5^\circ$ and $\varphi = 0$, we generated $|\phi^+\rangle$ Bell states with an initial concurrence of 0.90 ± 0.01. Either one or both photons were transmitted through the two types of channels, as described before. For each decoherence setting, the output state concurrence is calculated from the reconstructed density matrix. It is presented in Fig. 3 as a function of the noise probability P, along with the theoretical predictions. When either the two-field or the isotropic channels are applied to one of the two qubits, the concurrence is degrading similarly as a linear function of P. Entanglement breaking should occur when $P = \frac{1}{2}$. Reconstructed processes of the measured entanglement breaking points are presented in Fig. 4 using the Bloch sphere representation: A two-field process of $P = 0.52 \pm 0.01$ is shown in Fig. 4(a), and an isotropic process of $P = 0.59 \pm 0.01$ is shown in Fig. 4(b). According to theoretical calculations, if the channels are applied to both qubits, the concurrence dynamics is quadratic with P. Here, for the two processes, the dynamics is close but not identical. Entanglement breaking for the two-field channel occurs when $P = \frac{1}{3}$, and for the

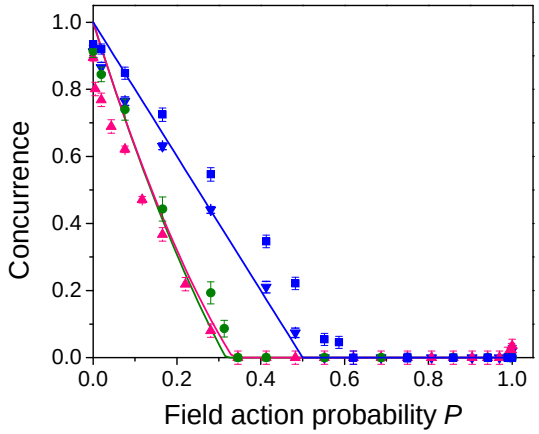

FIG. 3. (color online) Measured entanglement dynamics of a $|\phi^+\rangle$ state. Four cases are presented: The two-field channel, when applied to one photon (downward blue triangles) or to both (upward pink triangles), and the isotropic channel, when applied to one photon (blue squares) or to both (green circles). Solid lines represent the theoretical predictions.

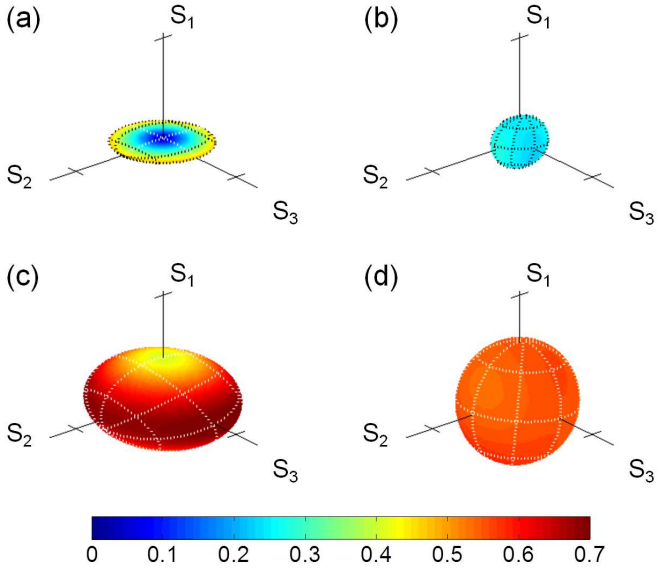

FIG. 4. (color online) Reconstruction of the measured entanglement breaking processes in the Bloch sphere representation. (a) and (b) correspond to the two-field and the isotropic channels when applied to only one of the photons, respectively. (c) and (d) represent the cases when the two-field and the isotropic channels are applied to both photons, respectively. Ellipsoid surface colors show the distance from the origin. Axis ticks are at values of 1.

isotropic channel when $P = \frac{3-\sqrt{3}}{4} \simeq 0.317$, which corresponds to a mapped sphere with a radius of $R = \sqrt{\frac{1}{3}}$. The corresponding measured processes for the two-field channel ($P = 0.31 \pm 0.01$), and for the isotropic channel ($P = 0.35 \pm 0.01$) are presented in Fig. 4(c) and Fig. 4(d), respectively.

As predicted, when the channels are applied to both photons, concurrence vanishes faster than when applied to one. The deviation from theory is larger for the isotropic channel, where decoherence is slower than expected. We explain this as a result of insufficient temporal separation by the birefringent crystals [18, 19, 21]; The coherence time of 300 fs is determined by the 3 nm wide bandpass filters that were used for spectral filtering. The two-field channel is using two 2 mm wide calcite crystals. On the other hand, the four-crystal configuration for the isotropic channel requires a different width for two of the crystals. Thus, we also used in this case two 1 mm crystals that reduced and delayed the decoherence effects.

V. DYNAMICS OF INITIAL PARTIALLY ENTANGLED STATES

In addition to studying the dynamics of initial maximally entangled states, we investigated the evolution of partially entangled states (PES). We now focus on the case of an isotropic channel which is applied only to one of the qubits. Two different classes of initial states were considered: pure PES and mixed PES. Different pure PES are generated by adjusting the HWP angle δ, so that the crystals are not equally pumped. The initial state concurrence is $C = \sin(4\delta)$. Specifically, we applied isotropic noise to states with initial concurrence of 0.50 ± 0.01 and 0.16 ± 0.01. When applied to pure PES, the concurrence dynamics should evolve according to the factorization law, derived by Thomas *et al.* [7]:

$$C[(I \otimes \$)\hat{\rho}] = C[(I \otimes \$)|\phi^+\rangle\langle\phi^+|]C(\hat{\rho})\,. \qquad (10)$$

This relation states that the concurrence of any initial pure state after the application of a channel \$ on one of the qubits can be factorized into the initial state concurrence and the concurrence that results when the same channel is applied to a pure Bell state.

The results for the initially pure PES are presented in Fig. 5(a), along with the corresponding dynamics of an initial $|\phi^+\rangle$ state that also appears in Fig. 3. The solid line in Fig. 5(a) represents a linear fit for the measured dynamics of the $|\phi^+\rangle$ state. As was stated before, theory predicts a linear dependency, and entanglement breaking at $P = 0.5$. Because of experimental errors, the concurrence fit reaches zero only at $P = 0.62 \pm 0.02$. From Eq. (10) it is clear that also the concurrence of the pure PES should have a linear dependency on P. We draw the straight dashed lines that connect the initial state concurrence at $P = 0$ and the experimental entanglement breaking point. As can be seen in Fig. 5(a), the dynamics of the two PES indeed follows the corresponding linear predictions, reaching zero concurrence at the same point.

We also studied initial PES that are partially mixed. The entanglement evolution of such states was derived as an extension to Eq. 10 by Jiménez-Farías *et al.* [8]. The

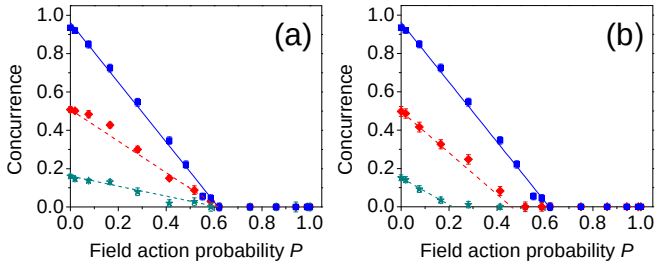

FIG. 5. (color online) Experimental results of the entanglement dynamics when the isotropic channel is applied to one qubit of initially (a) pure and (b) mixed PES.

initial mixed PES $\hat{\rho}$ is expressed in terms of an additional channel \$′ that is applied on one qubit of a pure two-qubit state $\hat{\sigma}$ which is not necessarily maximally entangled: $\hat{\rho} = (I \otimes \$')\hat{\sigma}$ [22]. The concurrence of $\hat{\rho}$ after a \$ channel is applied to one of its qubits is

$$C[(I \otimes \$)\hat{\rho}] = C[(I \otimes \$\$')|\phi^+\rangle\langle\phi^+|]C(\hat{\sigma})\,. \qquad (11)$$

Mixed PES were generated by introducing partial dephasing to an initial $|\phi^+\rangle$ state as follows: the compensating birefringent crystal was replaced with shorter crystals that did not correct sufficiently the temporal walk-off between the horizontal and the vertical amplitudes of the initial state, effectively generating a dephasing noise [9, 18]. in our case, where \$′ is a dephasing channel, and \$ is an isotropic channel, the concurrence also has a linear dependency on the isotropic noise probability P. Compared to the former case of initial pure states, decoherence occurs faster. As the initial state is more dephased, it will lose its entanglement earlier.

The experimentally measured dynamics of two initially mixed PES with initial concurrence of 0.50 ± 0.03 and 0.15 ± 0.01 is presented in Fig. 5(b), together with the $|\phi^+\rangle$ previous results. The initial concurrence values are similar to those that were studied in the pure PES case. The solid straight line is the same fit to the $|\phi^+\rangle$ case as with the pure PES case. The theoretical lines for the other two cases were calculated numerically for the concurrence values of the initially mixed PES. The presented dashed lines are corrected according to the experimental deviation of the $|\phi^+\rangle$ case, i.e., their P values are multiplied by the ratio 0.62/0.5 between the measured and predicted P values for entanglement breaking.

The presented results demonstrate that the entanglement contained in mixed PES is more fragile to noise compared to that of pure PES with the same level of concurrence. As in the case of maximally entangled states (Fig. 3), most of the experimental deviation from theory is explained by the length of the shortest crystals of the isotropic channel. Additional deviation in the PES case results from the overlap between the temporal modes of the initial dephasing channel and those created by the isotropic channels. Nevertheless, our results demonstrate the differences between the various cases very clearly.

VI. CONCLUSIONS

In this work, we studied the dynamics of entangled states when subjected to unital noisy channels. We showed that concurrence, as an entanglement measure, is linked in a simple way to the principal radii of the ellipsoid that represent the noise map in the Bloch sphere picture. Explicitly, when the channel is applied on one of the qubits, the concurrence is linear with the sum of the absolute values of the ellipsoid radii. We derived the concurrence for the case when the same Pauli channel is applied to both qubits, and found that it has a similar dependence, but with the sum of the squares of the ellipsoid radii.

We realized two different channels using birefringent crystals. These channels were applied to either one or to both photons of a polarization entangled photon pair, in order to experimentally demonstrate the entanglement dynamics of maximally entangled polarization states. In the case of isotropic noise that is applied to one of the photons, we also compared the entanglement degradation of initially pure and mixed partially entangled states. For states of similar initial concurrence, we have shown that dynamics depend on the initial degree of mixedness.

Two interesting issues that we leave open are the generalization of these results to non-unital channels and for systems of higher dimensionality. One may speculate: suppose a known unital channel operates on a maximally entangled three-qubit state. Can we quantify the entanglement of the output state using an entanglement measure which is proportional to the sum of the cubes of the ellipsoid radii that describe this channel?

ACKNOWLEDGMENTS

We thank the Israeli Ministry of Science and Technology for financial support.

[1] M. A. Nielsen and I. L. Chuang, *Quantum Computation and Quantum Information* (Cambridge University Press, Cambridge, U.K., 2000).

[2] K. Życzkowski, P. Horodecki, M. Horodecki and R. Horodecki, *Dynamics of Quantum Entanglement*, Phys. Rev. A, **65**, 012101(2001).

[3] T. Yu and J. H. Eberly, *Finite-Time Disentanglement via Spontaneous Emission*, Phys. Rev. Lett. **93**, 140404 (2004).

[4] P. J. Dodd and J. J. Halliwell, *Disentanglement and Decoherence by Open System Dynamics*, Phys. Rev. A **69**, 052105 (2004).

[5] A. Cabello, A. Feito, and A. Lamas-Linares, *Bell's Inequalities with Realistic Noise for Polarization-Entangled Photons*, Phys. Rev. A **72**, 052112 (2005).

[6] G. Puentes, A. Aiello, D. Voigt and J.P. Woerdman, *Entangled Mixed-State Generation by Twin-Photon Scattering*, Phys. Rev. A **75**, 032319 (2007).

[7] K. Thomas, F. de Melo, M. Tiersch, Ch. Kasztelan, A. Aragão, and A. Buchleitner, *Evolution Equation for Quantum Entanglement*, Nature Phys. **4**, 99 (2008).

[8] O. J. Fariás, C. L. Latune, S. P. Walborn, L. Davidovich, and P. H. S. Ribeiro, *Determining the Dynamics of Entanglement*, Science **324**, 1414 (2009).

[9] J.-S. Xu, C. F. Li, X.-Y. Xu, C. H. Shi, X. B. Zou, and G. C. Guo, *Experimental Characterization of Entanglement Dynamics in Noisy Channels*, Phys. Rev. Lett. **103**, 240502 (2009).

[10] T. Yu and J. H. Eberly, *Quantum Open System Theory: Bipartite Aspects*, Phys. Rev. Lett. **97**, 140403 (2006).

[11] M. P. Almeida, F. de Melo, M. Hor-Meyll, A. Salles, S. P. Walborn, P. H. S. Ribeiro, and L. Davidovich, *Environment-Induced Sudden Death of Entanglement*, Science **316**, 579 (2007).

[12] M. B. Ruskai, *Qubit Entanglement Breaking Channles*, Rev. Math. Phys. **15**, 643 (2003).

[13] M. Ziman and V. Bužek, *Concurrence versus Purity: Influence of Local Channels on Bell States of Two Qubits*, Phys. Rev. A **72**, 052325 (2005).

[14] S. N. Filippov, T. Rybár, and M. Ziman, *Local Two-Qubit Entanglement-Annihilating Channels*, Phys. Rev. A **85**, 012303 (2012).

[15] W. K. Wootters, *Entanglement of Formation of an Arbitrary State of Two Qubits*, Phys. Rev. Lett. **80**, 2245, (1998).

[16] C. King and M. B. Ruskai, *Minimal Entropy of States Emerging from Noisy Quantum Channels*, IEEE Trans. Inf. Theory **47**, 192 (2001).

[17] J. B. Altepeter, E. R. Jeffrey, and P. G. Kwiat, in Adv. At. Mol. Opt. Phys. **52**, 105 (2005).

[18] P. G. Kwiat, A. J. Berglund, J. B. Altepeter, and A. G. White, *Experimental Verification of Decoherence-Free Subspaces*, Science **290**, 498 (2000).

[19] A. Shaham and H. S. Eisenberg, *Realizing Controllable Depolarization in Photonic Quantum-Information Channels*, Phys. Rev. A **83**, 022303 (2011).

[20] A. Shaham and H. S. Eisenberg, *Quantum Process Tomography of Single-Photon Quantum Channels with Controllable Decoherence*, Phys. Scr. **T 147**, 014029 (2012).

[21] A. Shaham and H. S. Eisenberg, *Realizing a Variable Isotropic Depolarizer*, Opt. Lett. **37**, 2643 (2012).

[22] R. F. Werner, in *Quantum Information-An Introduction to Basic Theoretical Concepts and Experiments*, G. Alber *et al.*, Eds. (Springer, Berlin, 2002).